ACS Catalysis

Research Article

pubs.acs.org/acscatalysis

Enhanced Fe_2O_3 Reducibility via Surface Modification with Pd: Characterizing the Synergy within Pd/Fe Catalysts for Hydrodeoxygenation Reactions

Alyssa J. R. Hensley,[†,+] Yongchun Hong,[†,‡,§,+] Renqin Zhang,[†] He Zhang,[†] Junming Sun,[†] Yong Wang,*[,†,‡] and Jean-Sabin McEwen*[,†,∥,⊥]

[†]The Gene & Linda Voiland School of Chemical Engineering and Bioengineering, [∥]Department of Physics and Astronomy, and [⊥]Department of Chemistry, Washington State University, Pullman, Washington 99164, United States

[‡]Institute for Integrated Catalysis and [§]Environmental Molecular Sciences Laboratory, Pacific Northwest National Laboratory, Richland, Washington 99352, United States

Supporting Information

ABSTRACT: The synergistic catalysis in the hydrodeoxygenation of phenolic compounds over a Pd/Fe bimetallic surface has been well established. However, the nature of this synergy is still in part a mystery. In this work, we used a combined experimental and theoretical approach to understand a potential function of the surface Pd in the reduction of Pd/Fe_2O_3. This function of Pd was investigated via the comparison of the reduction properties as well as other physicochemical properties of samples synthesized by the reduction of Fe_2O_3 nanoparticles with and without surface Pd. Temperature-programmed reduction studies demonstrated the remarkable facilitation of reduction by addition of Pd, evidenced by a 150 °C shift toward lower temperature of the reduction peak of Fe^{3+}. From X-ray photoelectron spectroscopy and theoretical calculation results, the interaction between Pd and the Fe_2O_3 surface occurs through the exchange of electrons with both the surface Fe and O atoms. This bonding between the Pd and surface oxide elements causes the Pd to partially donate electrons to the oxide surface, making the surface electrons more delocalized. This electron delocalization stabilizes the reduced oxide surfaces, as suggested by the TPR results and theoretical prediction. Therefore, the stabilization of the reduced Fe surface as well as the facilitated water formation by introduction of Pd is expected to significantly contribute to the Pd−Fe synergy in hydrodeoxygenation catalysis.

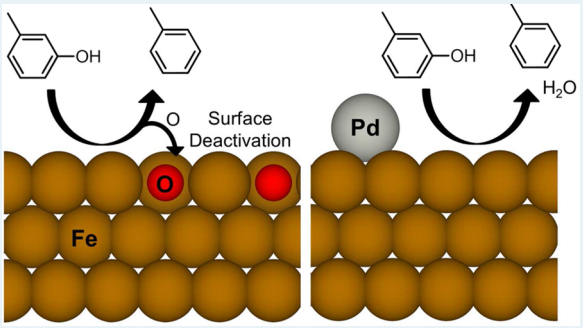

KEYWORDS: *bimetallic catalysts, biomass conversion, hydrodeoxygenation, Pd−Fe, density functional theory, oxide doping effects, enhanced oxide reduction*

1. INTRODUCTION

As traditional fuel sources are depleted in this ever more industrial world, the need for renewable and sustainable fuel alternatives rises.[1] A particularly promising replacement for transportation fossil fuels are biofuels,[2] which are carbon neutral, nearly SO_x-free and generate ∼50% less NO_x emissions than traditional diesel oil.[3] One method of producing biofuels is through the pyrolysis of biomass to bio-oils and successive refinery of bio-oils, and this process has been identified as the most cost-effective approach.[4] The key issue in the bio-oil upgrading is to efficiently reduce their high oxygen content (∼20−40 wt %) to less than 2 wt % for fuel applications. The oxygenates in bio-oils mainly exist in the form of acetic acid, furans, ketones, and phenolics,[3] which are corrosive, thermally unstable, and highly viscous.[5] The removal of oxygen in these bio-oils can be achieved in a similar manner with the hydrodesulfurization (HDS) and hydrodenitrogenation (HDN) processes in petroleum industry, i.e., removing oxygen in the form of water in hydrodeoxygenation (HDO) process.

Among those major components, phenolic compounds derived mainly from the pyrolysis of lignin have much lower oxygen content and are more readily convertible to hydrocarbon fuels. The catalytic HDO of lignin derived bio-oils and their representative compounds (guaiacol, cresols, anisole, etc.) were intensively investigated in the past decade.[6−11] Fe based catalysts were found to be promising for the HDO of lignin derived compounds for their high C−O bond cleavage selectivity toward the production of aromatics.[12−14] The limited gasification and ring-saturation selectivity on Fe catalysts ensures better atomic economics for carbon and hydrogen. Furthermore, the addition of Pd in the carbon supported Fe catalyst leads to a synergic catalysis with increasing activity toward aromatics production.[14] Our preliminary theoretical calculations showed that the Fe is the

Received: December 16, 2013
Revised: July 21, 2014

   dx.doi.org/10.1021/cs500565e | ACS Catal. 2014, 4, 3381−3392

active phase for the HDO reaction as the Fe surface produces a greater distortion of the C−O bond in adsorbed phenol[14] and the Pd−Fe interactions shift the Pd's d-band center away from the Fermi level and thereby impedes the adsorption of aromatics.[15]

The question remains as to what roles the Pd plays in the Pd/Fe catalyst. The first possibility is that, while the Fe's electronic structure remains unaffected by the Pd−Fe interactions, the changed electronic structure of the Pd dopant could cause a general weakening of the adsorption strength of reaction intermediates and products which will eventually increase the reaction rate by facilitating product desorption[16] and/or alter the favorable reaction mechanism by altering the adsorption configuration.[17] The second possibility is that as Pd single crystal surfaces have been shown to have a significantly higher sticking coefficient for H_2 relative to Fe single crystal surfaces,[18] the Pd acts as the H_2 activation site for the HDO reaction. The third possible function of Pd in the Pd/Fe bimetallic catalyst is in its greater potential for promoting the formation of water over the Fe surface,[19] preventing the metallic Fe surface from being oxidized by surface oxygen species. The fourth possible function of Pd in the Pd/Fe catalyst, and the function examined here, is that the Pd protects the Fe surface from deactivation by water oxidation by stabilizing the reduced Fe surface through the Pd−Fe electronic interactions.

The active metallic Fe has been shown to be highly susceptible to oxidation by surface oxygen species and thus easily poisoned.[13] It is critical to remove the surface oxygen species in the form of water to maintain a metallic Fe surface. It was well-documented that the reducibility of an oxide can be significantly affected by various base metal dopants, as shown for CeO_2,[20,21] La_2O_3,[22] TiO_2[23] systems, as the dopant will weaken the bonds holding the surface oxygen in place.[21,23,24] Other explanations of the dopant effect focus on the dopant's ability to facilitate H_2 dissociation and associated H_2 spillover.[25−27]

In this work, the effect of Pd doping on the reducibility of Fe_2O_3 and its catalytic consequences on the HDO of phenolics over the reduced Pd/Fe bimetallic catalysts was investigated via a combined experimental and theoretical approach. Here, we show that the Pd in the Pd/Fe catalyst acts as a dopant that protects the Fe surface from oxidation through the electronic stabilization of the reduced metal surface, weakening the surface oxygen bonds, and by promoting the formation of water. The mechanism of how the surface oxygen bond weakening occurs in the Pd on Fe_2O_3 system will be discussed based on DFT calculations and experimental observations.

2. METHODS

2.1. Preparation of Fe_2O_3 Sample. The Fe_2O_3 sample was prepared by an aqueous phase precipitation of ferric nitrate ($Fe(NO_3)_3\bullet 9H_2O$, Sigma-Aldrich, ≥99.999%) with ammonium carbonate ($(NH_4)_2CO_3$, Sigma-Aldrich, 99.999%) at room temperature, and the pH of the resulting solution was fixed at ∼8.[28] The precipitate was collected via filtration and then washed six times with a significant amount of deionized water. The obtained solids were then dried in an oven (80 °C) overnight, meshed, and then calcined in an oven at 400 °C for 5 h.

2.2. Preparation of Pd/Fe_2O_3 Samples. The Pd/Fe_2O_3 samples with different Pd loadings (0.1−5 wt %) were prepared using incipient wetness impregnation. In a typical synthesis process, $Pd(NH_3)_4(NO_3)_2$ aqueous solution (Sigma-Aldrich, 10 wt %) was diluted to a certain concentration (0.1 M for 5 wt % sample) with deionized water and then added onto the as-prepared Fe_2O_3 powder. After impregnation, the resulting samples were dried in an oven (80 °C) overnight, meshed, and then calcined in flowing N_2 (50 mL/min, STP) at 350 °C (ramping rate = 5 °C/min) for 2 h. The resulting samples were denoted as mPd/Fe_2O_3, with m indicating the loading of Pd.

2.3. Preparation of 5Pd/C Catalyst. The Pd/C sample with 5 wt % Pd loading (denoted as 5Pd/C) was prepared by incipient wetness impregnation.[14] A desired amount of $Pd(NH_3)_4(NO_3)_2$ (Sigma-Aldrich, 99.99%) aqueous solution was added to a TA70 carbon (1290 $m^2\ g^{-1}$, Pico Inc.) support. After impregnation, the resulting catalyst was dried in an oven (80 °C) overnight and then calcined in flowing N_2 (50 mL/min, STP) at 350 °C (ramping rate = 5 °C/min) for 2 h.

2.4. Characterizations. N_2 adsorption−desorption isotherms were recorded by a TriStar II 3020 automatic physisorption analyzer at 77 K. Samples were degassed in vacuum at 200 °C for 1 h before characterizations. The specific surface areas were evaluated using the Brunauer−Emmett−Teller (BET) equation,[29] while the pore volume and diameter data were calculated based on the Barrett-Joyner-Halenda (BJH) equation using the desorption branch.[30]

Transmission electron microscopic (TEM) images were collected on a Philips CM-200 platform operated at 200 kV. Samples were meshed and dispersed in ethanol under ultrasonic agitation before loading on the support grids.

Temperature programed reduction (TPR) experiments were performed on an AutoChem II 2920 chemisorption analyzer. Samples were *in situ* pretreated with flowing He (50 mL/min, STP) at 350 °C for 0.5 h before TPR tests. After cooling down to room temperature in flowing He (50 mL/min, STP), samples were purged with 10 vol % H_2 (balanced with Ar) for 15 min and then heated to 900 °C (ramping rate = 5 °C/min) and kept for 20 min. The effluent gas flowed through a cold trap cooled in an ice-salt bath to remove the moisture before being analyzed by a thermal conductivity detector (TCD), and the H_2 consumption was calibrated using quantitative reduction of a standard Ag_2O sample.

X-ray photoelectron spectroscopy (XPS) measurements of Pd/Fe_2O_3 samples were performed on a Physical Electronics Quantum 2000 Scanning ESCA microprobe equipped with a focused monochromatic Al Kα X-ray (1486.7 eV) source, a spherical section analyzer, and an attached catalytic side chamber. The binding energy values are referenced to the contamination carbon (C 1s) at 285.00 eV.

X-ray diffraction (XRD) patterns were collected on a Philips X'pert MPD (Model PW 3040/00) equipped with a Cu Kα (incident wavelength λ = 0.15406 nm) X-ray source operating at 40 kV and 50 mA. A step-size of 0.04 and accumulation time of 1.6 s was used during the scanning. The obtained patterns were analyzed using the MDI Jade 6 software with JCPDS. Reduced samples (denoted as 1Pd/Fe_2O_3-300) were prereduced in flowing H_2 (50 SCCM) at 300 °C for 2 h and then passivated with flowing 1 vol % O_2 (balanced with N_2) at room temperature for 12 h. Fresh samples were tested without any pretreatment.

2.5. Computational Details. The Vienna *Ab Initio* Simulation Package (VASP)[31,32] was used for all theoretical calculations. As metal oxides are known to exhibit strong on-site Coulombic interactions, we employed the method of DFT +U[33] where the U parameter can be tuned so that the

dx.doi.org/10.1021/cs500565e | ACS Catal. 2014, 4, 3381−3392

calculated bulk parameters of the oxide (e.g., lattice size, magnetic moments, band gap, etc.) match with experimental results. The method of Dudarev et al.[34] was used to include the DFT+U corrections with the Coulomb and screened exchange parameters (U, J) set to 5 and 1 eV, respectively.[33,35] These parameters were thoroughly screened and optimized by Rollmann et al.[33] for the α-Fe_2O_3 system and are frequently used in the literature.[35−39] These DFT+U parameters were applied to the d-states of the Fe and p-states of the O in the oxide and not to the adsorbing Pd as the Fe and O composing the oxide surface should experience similar strong on-site Coulombic interactions.

The projected augmented wave (PAW)[40] method was employed for the electron−ion interactions and the generalized gradient approximation (GGA) through the Perdew−Wang-91 (PW91)[41] functional accounted for the electron exchange-correlation effects. The plane wave basis set was expanded to a kinetic energy of 450 eV and spin polarization effects were employed to correctly account for the ferromagnetic nature of Fe. The interpolation for the electron correlation was performed using the method of Vosko et al.[42] which enhances the magnetic moments and magnetic energies of the system. Supercell **k**-points sampling was performed in these systems using the Monkhorst−Pack[43] method and grids of (6 × 6 × 3) and (6 × 6 × 1) were used for the bulk and surface systems, respectively, while the grid was increased to (12 × 12 × 1) for electronic analyses of the surfaces. Gaussian smearing[44] of 0.1 eV was used for the structural relaxations and energy calculations, while the smearing width was decreased to 0.05 eV for electronic analyses, to improve convergence and the total energy was extrapolated to zero Kelvin. The total energy was converged to at least 10^{-4} eV for all systems, and each system was considered to be in equilibrium when the forces were less than 0.03 eV/Å.

Initially, the bulk α-Fe_2O_3 unit cell was studied to both verify the calculation parameters described above and determine the optimum lattice spacing. The α-Fe_2O_3 phase studied here also agrees well with the experimental XRD results which shows that the original Fe_2O_3 particles are in the α hematite phase. The volume of this unit cell was allowed to relax so as to minimize the total energy of the system, and the optimum lattice constants were found to be 5.059 and 13.828 Å, respectively, which compare well with both the literature values and experimentally determined lattice parameters.[33,35,38,39] Previous studies have shown that the most stable magnetic structure for α-Fe_2O_3 is an antiferromagnetic ordering with double Fe layers of spin up and spin down (++--).[33] This magnetic ordering was used in all calculations, and the resulting magnetic moment of the Fe in the bulk system was found to be 4.15 μ_B/Fe atom. This result also agrees well with the literature values[10,12,15] which also show that the addition of the on-site Coulombic interactions through the above DFT+U method results in a higher degree of agreement with experimental results.

For the near surface analyses of the adsorption of Pd and the formation of oxygen vacancies, the (0001) surface was chosen as it is known to be the natural growth face of α-Fe_2O_3.[45] Due to the complex and computationally demanding nature of the DFT+U calculations, these systems were modeled using p(1 × 1) supercells for the 0, 1/2, and 1 ML Pd covered α-Fe2O3 (0001) surfaces, while the 1/8 ML Pd coverage case was modeled using a p(2 × 2) supercell. As the supercell was increased to p(2 × 2), the **k**-points sampling grids were decreased to (3 × 3 × 1). All models contained 18 atomic substrate layers with symmetric surfaces in order to cancel out the dipole moments and dipole corrections were not used as both of the exposed surfaces had adsorbed Pd and oxygen vacancies, where applicable. All atoms were allowed to relax in these surface models, and the repeating surfaces were separated by ∼15 Å of vacuum. In the [0001] direction, the α-Fe_2O_3 surface can have four possible terminations depending upon the layering of the iron and oxygen within the near surface structure. Several studies have shown that the Fe−O_3−Fe terminated structure was the most energetically stable of the four possible structures, even under varying oxygen chemical potentials, and we have therefore chosen to study this termination.[12,13]

3. RESULTS AND DISCUSSION

3.1. Pd/Fe_2O_3 Surface Properties. *3.1.1. Texture Properties and Morphology of Pd/Fe_2O_3 Samples.* Texture properties of the Fe_2O_3 and Pd/Fe_2O_3 samples are listed in Table 1.

Table 1. Texture Properties of the Fe_2O_3 and Pd/Fe_2O_3 Samples

sample	A_{BET} (m^2/g)[a]	V_p (cm^3/g)[b]	d_p (nm)[c]
Fe_2O_3	40	0.18	16.2
0.1Pd/Fe_2O_3	43	0.19	15.0
1Pd/Fe_2O_3	44	0.18	14.8
5Pd/Fe_2O_3	41	0.17	15.2

[a]BET specific area. [b]Pore volume evaluated using BJH equation based on desorption branch. [c]Mean pore diameter evaluated using BJH equation based on desorption branch.

The Pd/Fe_2O_3 samples showed negligible differences compared with Fe_2O_3 support in terms of BET specific surface area, pore volume, and mean pore diameter. These negligible differences will not be taken into account in the following discussion of the effects of Pd addition to the Fe_2O_3 on its reducibility.

In addition, the amount of Pd required for 1 ML coverage was estimated based on the surface area of the Fe_2O_3 samples, assuming that the lattice constant of the Pd fcc structure to be 3.8907 Å. Based on this estimation, the loading of Pd required for 1 ML would be ca. 4.4 wt %, which is close to the highest Pd loading (5 wt %, denoted as 5Pd/Fe_2O_3) studied in this work. Representative TEM images, shown in Figure 1, show the 10−20 nm domain size of Fe_2O_3 and sub-5 nm sized Pd nanoparticles in the 5Pd/Fe_2O_3 sample. Apparently, even the sample with 5 wt % Pd featured a significant 3D structure, rather than a complete surface layer. Therefore, the actual coverage is expected to be much less than 1 ML for all Pd/Fe_2O_3 samples. It is expected that samples with lower Pd loading will lead to smaller Pd nanoparticles, as confirmed by the absence of Pd diffraction peaks in the XRD pattern (Figure 2).

3.1.2. Surface Characterization of Pd/Fe_2O_3 Samples. The effect that the presence of Pd has on the Fe_2O_3 surface has been investigated here via theoretical adsorption, partial density of states (PDOS), differential charge density, Bader charge analysis, and core level binding energy calculations along with experimental XPS studies. These studies quantify the method by which Pd both binds to and modifies the oxide surface.

To begin this analysis, all possible adsorption and coadsorption sites for surface Pd coverages of 1/2 and 1 ML were investigated from theory and are shown in Figure 3. These

dx.doi.org/10.1021/cs500565e | ACS Catal. 2014, 4, 3381−3392

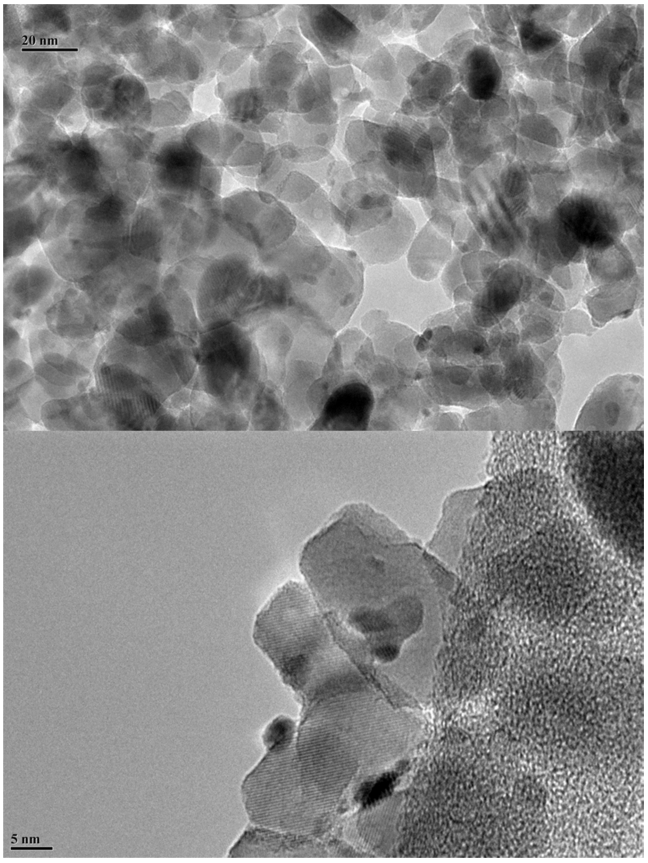

Figure 1. Representative TEM (accelerating voltage = 200 kV) images for 5Pd/Fe_2O_3 sample. The dark patches show the location of Pd on the sample.

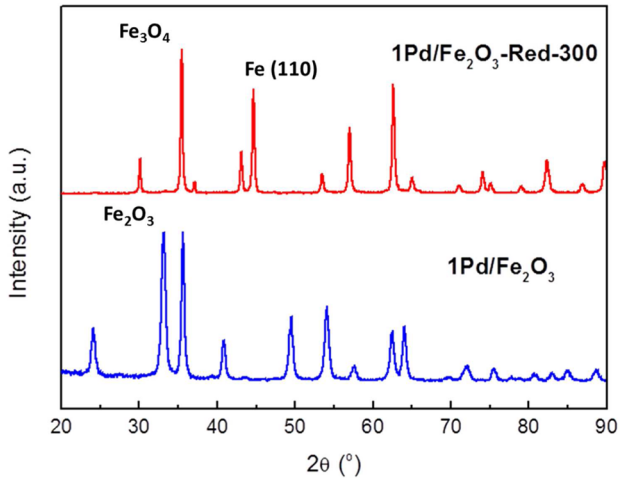

Figure 2. XRD patterns of fresh and reduced (in flowing 50 vol % H_2/N_2 at 300 °C) 1Pd/Fe_2O_3 samples measured with Cu Kα source operated at 40 kV and 50 mA.

coverages are achieved when first one and then two Pd atoms are adsorbed onto the (0001) surface in the p(1 × 1) unit cell as the α-Fe_2O_3 system has two distinct Fe atoms.

These various adsorption sites are identified by the Fe_2O_3 surface elements that the Pd is positioned above. For example, in the 1/2 ML coverage case, the Pd can adsorb atop three separate Fe atoms (Fe_1, Fe_2, and Fe_3) along with atop a surface oxygen (O_T), bridging two Fe atoms (Fe_B), bridging two oxygen atoms (O_B), and in a hollow site surrounded by surface oxygen atoms (O_H). Previous work done by Kiejna et al.[35] examined the adsorption of Pd on this same oxide surface using DFT; however, their study was limited to the Fe top sites for the 1/2 ML case and the Fe_1Fe_2 site for the 1 ML case. Our work here expands upon that work by studying all possible adsorption sites for both coverages. Each adsorption site was evaluated using the adsorption energy, as defined by

$$E_{Ads} = \frac{E_{Total} - E_{Surface} - N_{Pd}E_{Pd\ Atom}}{N_{Pd}} \quad (1)$$

where E_{Total}, $E_{Surface}$, and $E_{Pd\ Atom}$ are the energies of the total system, the α-Fe_2O_3 (0001) surface, and a single, gas phase Pd atom, while N_{Pd} is the total number of Pd atoms in the total system. When using this definition, a negative E_{ads} means that the adsorption is an exothermic process, and the resulting energies and Pd−O bond lengths for all possible Pd adsorption sites at the two coverages are presented in Table 2.

For both Pd coverages studied, the Pd preferentially adsorbs onto the α-Fe_2O_3 (0001) surface through oxygen dominant sites as evident by the adsorption energies. For the 1/2 ML case, the strongest adsorption energy occurs when the Pd adsorbs into the O_B site followed by the O_T and Fe_1 sites. These sites all have similar Pd−O bond lengths, while the additional Fe top sites show both a significant increase in the Pd−O bond length and decrease in the adsorption energy. This trend continues for the 1 ML Pd case as the O_TO_T site is the most favored adsorption site with the smallest Pd−O bond distance. In addition to the above results, the adsorption energies for the Fe_1, Fe_2, Fe_3, and Fe_1Fe_2 sites agree well with those presented by Kiejna et al.[35] Also, it is clear that the adsorption energy per Pd atom significantly increases with Pd coverage. This shows that the Pd−Pd lateral interactions are attractive and that the formation of bulk Pd patches on the Fe_2O_3 surface is favorable, which is in good agreement with the experimental TEM images (Figure 1).

The electronic effect of the adsorption of Pd on the α-Fe_2O_3 (0001) surface was first examined using the electron density difference, as calculated by

$$\Delta\rho = \rho_{Total} - \rho_{Surface} - \rho_{Pd} \quad (2)$$

where ρ_{Total}, $\rho_{Surface}$, and ρ_{Pd} are the charge densities of the total system, the clean α-Fe_2O_3 (0001) surface, and the adsorbing Pd in the same unit cell. This analysis allows us to visualize how the valence electrons in the system have transferred upon the adsorption of Pd at the 1/2 and 1 ML coverages, as shown in Figure 4.

The adsorption of Pd under both coverages appears to have similar electron exchange with the surface where the Pd and surface Fe significantly exchange electrons with more minor electron exchanges between the adsorbing Pd and surface oxygen. This electron exchange was verified by examining the PDOS for the surface Fe's d-orbital, the O's p-orbital, and the Pd's d-orbital. The PDOS for each of the above-mentioned elements in the 0, 1/2, and 1 ML Pd coverage cases are shown in Figure 5a. The Fe PDOS shown for all systems in Figure 5 is the Fe(+1) atom (see Figure 3) as the differential charge density results show the bonding between the Pd and Fe in the oxide surface to be exclusively with the Fe(+1) atom. For the oxygen PDOS, the oxygen in the clean Fe_2O_3 surface were all found to be equivalent, while the surfaces with adsorbed Pd showed a slight electronic difference between the surface

dx.doi.org/10.1021/cs500565e | ACS Catal. 2014, 4, 3381−3392

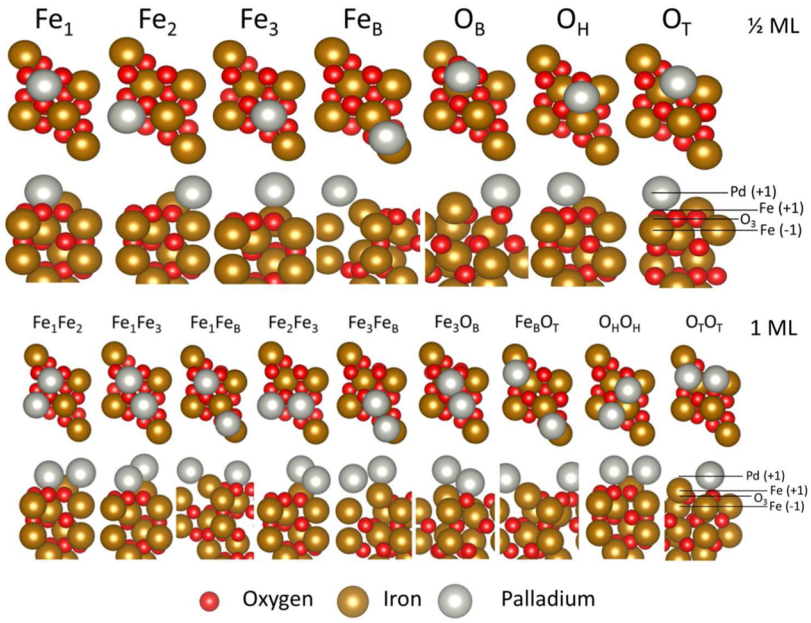

Figure 3. All possible adsorption configurations for Pd on the α-Fe_2O_3 (0001) surface at Pd coverages of 1/2 and 1 ML. These sites are defined based on the adsorbing Pd's relation to the surface Fe and O (e.g., Fe_1, Fe_2, and Fe_3 all have Pd adsorbing atop a surface Fe atom while the O_B site has Pd bridging two surface O atoms). The various oxide layers are labeled as Fe (+1), O_3, and Fe (−1) with the O_3 layer as the reference with the Fe (±1) being either above or below that layer, respectively. Also, the adsorbing Pd is labeled as Pd (+1).

Table 2. Adsorption Energies and Pd−O Bond Length for Pd in All Possible Adsorption Sites on the α-Fe_2O_3 (0001) Surface for Coverages of 1/2 and 1 ML[a,b]

sites	E_{Ads} (eV/Pd)	d_{Pd-O} (Å)
1/2 ML Pd		
Fe_1	−1.59	2.26
Fe_2	−1.34	2.42
Fe_3	−0.99	3.05
Fe_B	unstable	
O_B	−1.69	2.23
O_H	unstable	
O_T	−1.66	2.08
1 ML Pd		
Fe_1Fe_2	−2.09	2.35, 2.62
Fe_1Fe_3	−2.27	2.37, 3.39
Fe_1Fe_B	unstable	
Fe_2Fe_3	−2.13	2.50, 3.38
Fe_3Fe_B	−2.19	3.27, 2.55
Fe_3O_B	unstable	
Fe_BO_T	unstable	
O_HO_H	unstable	
O_TO_T	−2.30	2.12

[a]Adsorption energy, E_{Ads}, and Pd−O bond length, d_{Pd-O}. [b]Structures of each configuration are shown in Figure 3.

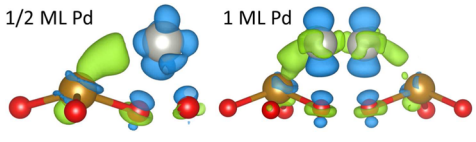

Figure 4. Electron transfer due to Pd adsorption on the α-Fe_2O_3 (0001) surface calculated via the electron density difference. The site examined for the 1/2 and 1 ML cases shown above were the O_B and O_TO_T sites (Figure 3), respectively. The isosurface level was set at 0.01 e/Å^3, and the green (blue) areas represent a gain (loss) of electrons.

oxygen atoms that were and were not bonded to the adsorbed Pd. Here, the oxygen PDOS shown is for the Pd bonded oxygen. It was also found that the Pd in the 1 ML coverage case were equivalent.

Initially, the α-Fe_2O_3 (0001) surface shows a strong semiconductor profile with a band gap of ∼2 eV which is consistent with previous theoretical and experimental results.[46,47] The adsorption of Pd on this surface at both coverages creates peaks in both the Fe and oxygen PDOS in the original band gap, and there is a significant overlap between both the Pd and Fe and the Pd and O valence states, supporting the electron exchange observed in Figure 4. Also, as the coverage of Pd on the surface is increased, the Pd d-states become more continuous and metallic in character.

Furthermore, we performed a Bader charge analysis[48] on the α-Fe_2O_3 (0001) surfaces with 0, 1/2, and 1 ML of Pd (the O_B and O_TO_T sites were studied for the 1/2 and 1 ML cases, respectively). The Bader charge results were fully converged relative to each system's fast Fourier transform (FFT) grid, and the change in the surface element's charge for the complete surfaces discussed above is relative to gas phase Pd and the clean α-Fe_2O_3 (0001) surface. These results are presented in the top half of Table 3. From these results, it is clear that the electron exchange between the adsorbing Pd and surface Fe is not completely equal. For the 1/2 ML case, the adsorbing Pd gains a partial positive charge due to the donation of ∼0.3 e to the adjacent surface Fe. This trend is consistent with the charge transfer observed for the 1 ML case, where each adsorbed Pd loses ∼0.1 e to the topmost Fe in the oxide surface.

Thus far, our theoretical results predict that the adsorption of Pd on the Fe_2O_3 surface will preferentially occur through oxygen sites with the adsorption energy increasing with a decrease in the Pd−O bond length. While Pd adsorbs strongest at oxygen sites, it is clear from our electronic analysis that the strong adsorption of Pd is due primarily to the exchange of electrons between the Pd and exposed Fe with minor electron

dx.doi.org/10.1021/cs500565e | ACS Catal. 2014, 4, 3381−3392

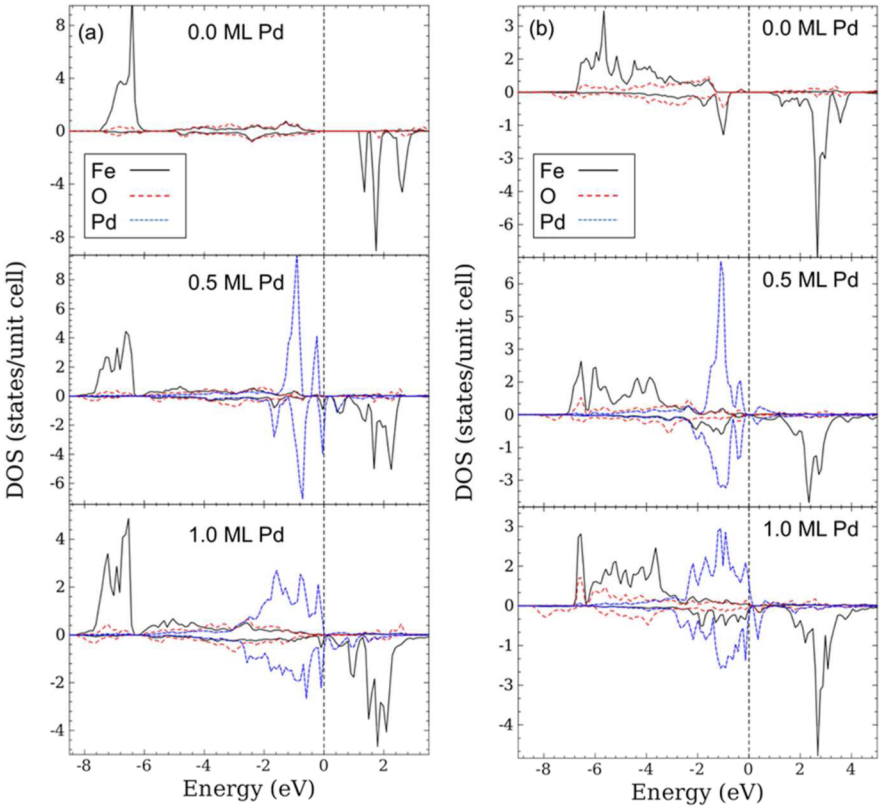

Figure 5. PDOS for the surface Fe's d-orbital, O's p-orbital, and Pd's d-orbital for the (a) complete α-Fe_2O_3 (0001) surfaces (O_B and O_TO_T adsorption sites used for the 1/2 and 1 ML coverages) and (b) α-Fe_2O_3 (0001) surfaces containing a single oxygen vacancy (O-2 site) with varying Pd coverages. The E_{Fermi} has been set to zero.

Table 3. Change in the Bader Charge (e) on the Surface Elements of the α-Fe_2O_3 (0001) Surfaces with Varying Pd Coverages[a]

Surfaces without Vacancies			
element	0.0 ML Pd	0.5 ML Pd	1.0 ML Pd
Pd (+1)		−0.3	−0.1
Fe (+1)	0.0	0.3	0.2
O_3	0.0	0.0	0.0
Fe (−1)	0.0	0.0	0.0
Single Oxygen Vacancy (O-2 Site)			
element	0.0 ML Pd	0.5 ML Pd	1.0 ML Pd
Pd (+1)		0.4	0.2
Fe (+1)	0.4	0.2	0.4
O_2	0.0	0.0	0.0
Fe (−1)	0.3	0.3	0.2

[a]The changes in the surface charges for the complete surfaces are relative to the gas phase Pd and the clean α-Fe_2O_3 (0001) surface, while the change in the surface charges for the single oxygen vacancy surfaces are relative to the Fe_2O_3 and Pd/Fe_2O_3 surfaces without vacancies. For the complete surfaces with 1/2 and 1 ML Pd coverages, the O_B and O_TO_T sites were studied, respectively.

exchange occurring between the adsorbing Pd and surface oxygen. In order to confirm the bonding between surface Fe and O with the adsorbing Pd predicted by theory, the surface electron status of Pd/Fe_2O_3 samples were characterized with XPS, and the resulting shifts in the spectra were compared to theoretically calculated core level binding energy shifts.[49,50] The detailed spectra for the unreduced Pd/Fe_2O_3 samples' Pd 3d, Fe 2p, and O 1s electrons are displayed in Figure 6.

The detailed spectrum in the Pd 3d region (Figure 6a) for the 5Pd/C sample shows the typical Pd 3d 5/2 binding energy value (335 eV) for metallic Pd.[51] Slight shifts toward higher binding energy were evident for the Pd 3d electrons in the Pd/Fe_2O_3 samples, especially for samples with high Pd loading (1 and 5 wt % Pd loading), compared with the 5Pd/C sample. The ca. 1 eV shift in the Pd 3d binding energy suggests that the Pd electron status is changed via the Pd−Fe_2O_3 interaction. For the spectra in the Fe 2p region (Figure 6b), a less distinct blue shift of ca. 0.1 eV can be found on the 5Pd/Fe_2O_3 sample compared with that of Fe_2O_3. This blue shift indicates that the Fe in the Pd doped Fe_2O_3 has a higher electron affinity, thus having a higher reducibility. A blue shift in the electrons in the Fe spectra means that the electrons bind more strongly to the Fe. In this case, the gain of electrons on the Fe is both more feasible and has been shown to be true from theory (Table 3), thus allowing the Fe to be more readily reduced. The binding energy for O 1s electron (Figure 6c) also shows a moderate blue shift (ca. 0.2 eV) for the Pd/Fe_2O_3 samples compared with Fe_2O_3, indicating a modification of the electron status of oxygen by addition of Pd. The blue shift in both the Pd and Fe XPS spectra indicates that we have no evidence of surface Pd−Fe alloy formation in the unreduced samples, and all the features of the Pd and Fe are likely modified by the presence of oxygen in the oxide.

We have calculated similar shifts in the core level binding energies for the above orbitals from theory on the 1/2 ML Pd covered α-Fe_2O_3 (0001) surface (O_B site), and the results are shown in Table 4 (additional calculation details presented in the Supporting Information). The DFT calculated core level binding energy shifts are in agreement with the experimental

dx.doi.org/10.1021/cs500565e | ACS Catal. 2014, 4, 3381−3392

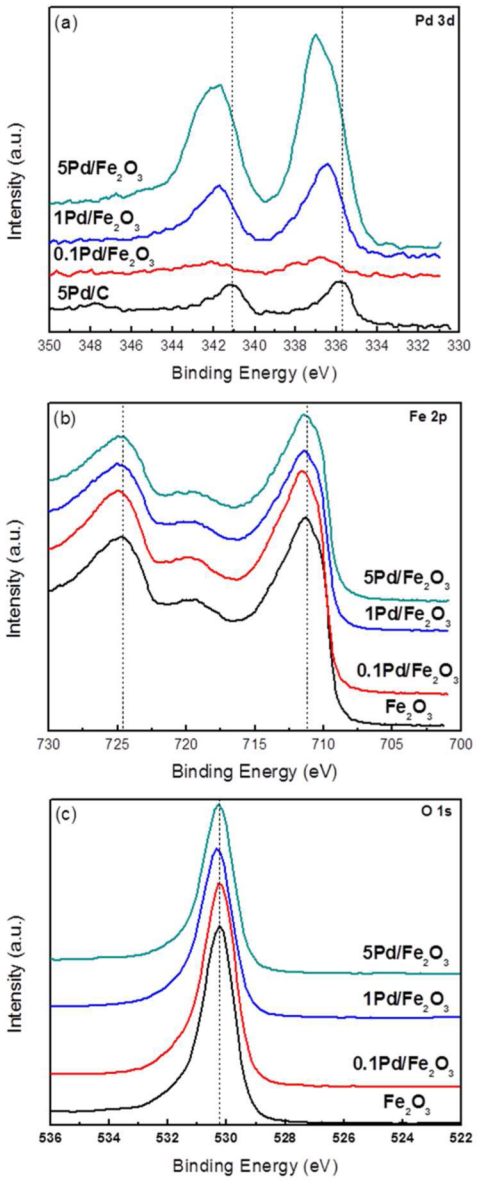

Figure 6. XPS spectra of fresh Pd/Fe_2O_3 samples in the Pd 3d (a), Fe 2p (b), and O 1s (c) regions measured with Al Kα source and calibrated with C_{1s} = 285.00 eV.

Table 4. Core Level Binding Energy Shifts for the Pd 3d, Fe 2p, and O 1s Electrons Calculated in the Pd/Fe_2O_3 System Relative to the Pd/C and Clean Fe_2O_3 Catalysts, Respectively[a]

excited electron	theory (eV)	experiment (eV)
Pd 3d	0.75	1.0
Fe 2p	0.51	0.1
O 1s	0.59	0.2

[a]Theoretical results calculated from the 1/2 ML Pd coverage system (site O_B) and experimental results calculated from the XPS spectra.

shifts determined from the XPS spectra with the major differences seen in the Fe 2p and O 1s shifts due to the higher Pd surface coverage seen theoretically (higher Pd−O and Pd−Fe interaction from theory). This confirms that the adsorption of Pd on the Fe_2O_3 surface results in bonding between Pd and surface Fe and Pd and surface O and that the subsequent electron exchange between the Pd and Fe and Pd and O results in the measured XPS energy shifts (Figure 6).

Overall, it is clear that the surface Pd both modifies the Fe_2O_3 surface's electronic structure and is in turn modified by the electronic interactions occurring within the surface and adsorbate. These interactions lead to a significant blue shift in the Pd 3d spectra with smaller blue shifts in the Fe 2p and O 1s spectra suggesting that the Fe in the oxide has a higher electron affinity and that electronic interactions occur between the Pd and both the Fe and O. The increased electron affinity on the surface Fe is also seen from the Bader charge analysis which shows that the surface Pd adsorption partially transfers electrons from the Pd adsorbate to the Fe oxide. This donation of electrons from the Pd to the surface partially delocalizes the electrons in the surface of the oxide, as can be seen in the PDOS by the appearance of Fe and oxygen states within the band gap. Also, as the Pd loading is decreased, the modification of Pd on the electron status of Fe and oxygen, as seen from XPS results, significantly decreases. This suggests that the influence of Pd will be restricted to its neighboring area. Therefore, the presence of Pd on the Fe_2O_3 surface delocalizes the surface electrons in the area surrounding the surface Pd which likely decreases the strong on-site Coulombic interactions (which are the cause of the band gap and electron localization within oxides) that occur between the surface Fe and oxygen, allowing the electrons to more freely transfer between the surface elements.

3.1.3. Reducibility of Pd/Fe_2O_3 Samples. Up until now, we have focused on characterizing the effect that surface Pd has on the Fe_2O_3 surface. Here, we present both experimental and theoretical results concerning the effect that surface Pd has on the reduction of the Fe_2O_3 surface in the form of TPR profiles and by creating oxygen vacancies within the model oxide surface with varying Pd coverages.

Figure 7 shows the TPR profiles of Pd/Fe_2O_3 and Fe_2O_3 samples. The peak (either negative or positive) at ca. 60−80 °C

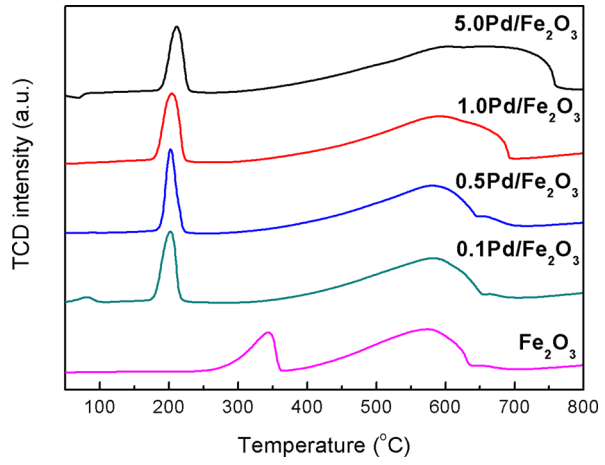

Figure 7. TPR profiles of the Pd/Fe_2O_3 samples. TCD signal was normalized by sample loading, recorded in 10 vol % H_2/Ar with ramping rate = 5 °C/min.

can be attributed to PdO_x reduction and/or PdH_x decomposition.[52] The two step reduction of Fe_2O_3 (Fe_2O_3 to Fe_3O_4 and Fe_3O_4 to Fe) was evident in all samples tested.[53] The overall chemical equations for the two major reduction steps are as follows:

dx.doi.org/10.1021/cs500565e | ACS Catal. 2014, 4, 3381−3392

$$1/2Fe_2O_3 + 1/6H_2 \rightarrow 1/3Fe_3O_4 + 1/6H_2O \quad (3)$$

$$1/3Fe_3O_4 + 4/3H_2 \rightarrow Fe + 4/3H_2O \quad (4)$$

Based on these equations, the ideal ratio of hydrogen atoms to reduce a single Fe atom (H/Fe) in the Fe_2O_3 system is 1/3, while the ideal H/Fe ratio in the Fe_3O_4 system is 8/3. The peak at low temperature (ca. 200 °C for Pd/Fe_2O_3 samples and 345 °C for Fe_2O_3 sample) was ascribed as reduction of Fe^{3+} to Fe^{2+} during the transformation of Fe_2O_3 to Fe_3O_4, as the H/Fe ratio for this peak is ca. 1/3 (Table 5), which is consistent with the reaction stoichiometric ratio of 1/3 for Fe_2O_3 reduction to Fe_3O_4. The peak at ca. 570 °C with a broad shoulder was assigned to the reduction of Fe_3O_4 to Fe. However, the reduction of Fe_3O_4 to Fe was not completed for all samples under TPR test conditions (10 vol % H_2 in Ar) for the low H_2 partial pressure as the H/Fe ratio for this peak (1.48−2.48 in Table 5) was less than its chemical stoichiometric ratio of 8/3.

Table 5. Quantitative TPR Analysis Results (Calibrated by Quantitative Reduction of Ag_2O Standard)

	zone 1		zone 2	
sample	peak temp (°C)	H/Fe	peak temp (°C)	H/Fe
Fe_2O_3	345	0.34	572	1.48
0.1 Pd/Fe_2O_3	202	0.32	582	1.75
0.5 Pd/Fe_2O_3	202	0.33	583	1.95
1.0 Pd/Fe_2O_3	203	0.35	590	2.17
5.0 Pd/Fe_2O_3	209	0.32	592	2.48

The doping of Pd on the surface of Fe_2O_3 shows two major changes in the TPR of the Fe_2O_3 surface. First, the reduction of Fe_2O_3 to Fe_3O_4 is significantly facilitated by the presence of surface Pd as seen in the temperature decrease from 345 °C on the clean Fe_2O_3 surface to ca. 200 °C on the Pd covered surfaces. Second, the reduction of Fe_3O_4 to Fe was enhanced by surface Pd as the H/Fe ratio was shown to increase with increasing Pd loading. These changes in the TPR results show that the presence of surface Pd facilitates the reduction of Fe_2O_3 to metallic Fe by reducing the temperature of the first reduction step and by promoting the overall formation of a greater amount of metallic Fe. Similar phenomena were extensively reported in the literature.[25−27,54,55] Most of the attention was paid to the Pd facilitated H_2 dissociation and associated H_2 spillover,[25−27] while the "intrinsic" aspect of the reducibility of oxides with dopants, i.e. the formation energy of oxygen vacancies, has been performed mainly from theory and with little experimental corroboration.[21−24] The creation of these oxygen vacancies has been shown to be essential in several catalytic reactions.[56−59]

This intrinsic effect of Pd on the reduction of Fe_2O_3 was investigated from theory by calculating the energetic and electronic changes to α-Fe_2O_3 (0001) surfaces with a single oxygen vacancy with the addition of Pd at coverages of 0, 1/2, and 1 ML. The possible oxygen vacancy sites in these surfaces were identified by examining the PDOS for the surface oxygen, and it was clear that the surface oxygen species in the clean Fe_2O_3 surface were all electronically equivalent while the Pd/Fe_2O_3 systems have two electronically different oxygen species. This difference in surface oxygen in the Pd/Fe_2O_3 surfaces is due to whether they are free or directly bonded to the adsorbing Pd and they have been designated O-1 and O-2, respectively. These possible oxygen vacancy sites in the complete α-Fe_2O_3 (0001) surfaces are identified in Figure 8.

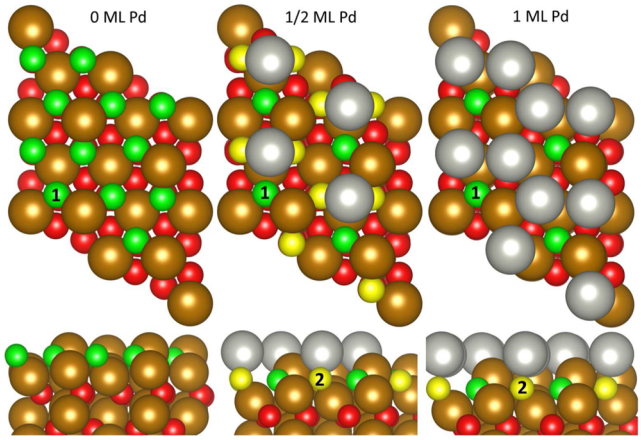

Figure 8. Possible oxygen vacancy sites in the α-Fe_2O_3 (0001) surface with Pd coverages of 0, 1/2, and 1 ML. The general color coding is as in Figure 3 with the different surface oxygen sites identified with either green (O-1) or yellow (O-2) spheres.

A single oxygen vacancy created at the O-1 and O-2 sites by the formation of water was modeled using the following chemical equation

$$n\text{Pd/Fe}_2\text{O}_3(s) + x\text{H}_2(g) \rightarrow n\text{Pd/Fe}_2\text{O}_{3-x}(s) + x\text{H}_2\text{O}(g) \quad (5)$$

where n is the number of surface Pd atoms, and x is the number of oxygen atoms removed from the surface layer. These systems were evaluated using the reaction energy as defined by

$$E_{rxn} = E_{products} - E_{reactants} = E_{n\text{Pd+Fe}_2\text{O}_{3-x}} + xE_{H_2O} - E_{n\text{Pd+Fe}_2\text{O}_3} - xE_{H_2} \quad (6)$$

where $E_{n\text{Pd+Fe}_2\text{O}_{3-x}}$, $E_{n\text{Pd+Fe}_2\text{O}_3}$, E_{H_2O}, and E_{H_2} are the energies for the system with a single oxygen vacancy, the complete surface, and gas phase water and hydrogen, and x is the number of oxygen removed from the surface. If E_{rxn} is negative, it means that the reaction which creates a surface oxygen vacancy and water from the Pd/Fe_2O_3 surfaces and hydrogen is exothermic and, therefore, energetically favorable. The energy required to purely break the bonds holding the surface oxygen in place is defined as the oxygen bond energy and is performed by fixing the position of all of the atoms in the nPd/Fe_2O_3 surface, removing a single oxygen, calculating the total energy of the fixed system, and determining the oxygen bonding energy using the following definition

$$E_{bond} = E^{fixed}_{n\text{Pd+Fe}_2\text{O}_{3-x}} + xE_{H_2O} - E_{n\text{Pd+Fe}_2\text{O}_3} - xE_{H_2} \quad (7)$$

where $E^{fixed}_{n\text{Pd+Fe}_2\text{O}_{3-x}}$ is the energy for the fixed system with a single oxygen vacancy. All other quantities are identical to those in eq 6. The calculated E_{bond} allows us to determine the relative energy required to break the oxygen free from the oxide surface to form a water molecule and provides a rough approximation of the energy barrier required to reduce the oxide surface as this calculated energy does not include any of the energy gained by the system due to the relaxation of the surface after the vacancy has been created but is purely a measure of the energy required to break the surface oxide bonds. The resulting oxygen bond

dx.doi.org/10.1021/cs500565e | ACS Catal. 2014, 4, 3381−3392

energy and reaction energy for vacancies created at the O-1 and O-2 sites for the three α-Fe_2O_3 (0001) surfaces (Figure 8) are shown in Figure 9.

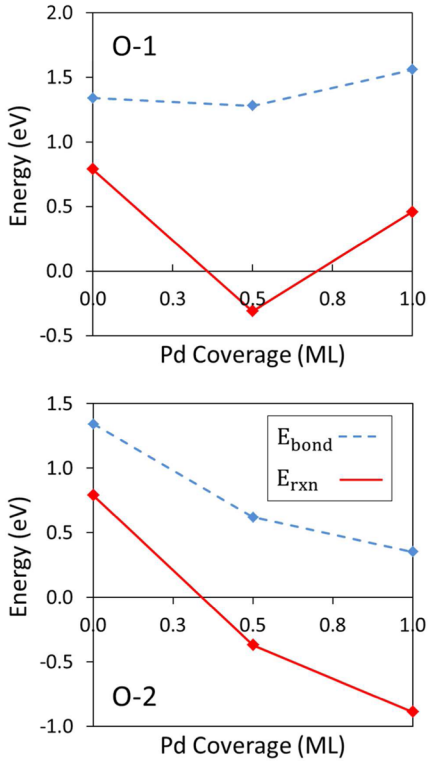

Figure 9. Energies of reaction (solid line) and oxygen bond (dashed line) for the creation of oxygen vacancies in α-Fe_2O_3 (0001) surfaces with increasing Pd surface coverage.

First, for an oxygen vacancy created at site O-1, it is clear the adsorption of Pd on the α-Fe_2O_3 (0001) surface decreases the reaction energy (E_{rxn}) by ~0.3 to 1.1 eV. For this free surface oxygen site, there is no overall trend in the reaction energy with Pd coverage as the initial 1/2 ML coverage sees a more significant drop in energy relative to the 1 ML coverage case. This result suggests that the addition of Pd to the Fe_2O_3 surface facilitates the reduction of that surface even when the Pd is not directly bonding with the oxygen being removed. Contrary to these results, as the Pd coverage increases, we see a slight increase in the energy required to purely break the bonds holding the oxygen in the surface (E_{bond}). These trends would appear to contradict each other as the E_{rxn} suggests that surface Pd promotes the creation of oxygen vacancies even when the Pd and oxygen are not bonding, while E_{bond} suggests the opposite effect. This contradiction is resolved by examining the overall stability of the surface using the surface energy defined by

$$E_{surf} = \frac{E_{Total} - N_{Fe_2O_3}E_{Bulk}^{Fe_2O_3} - N_{Pd}E_{Bulk}^{Pd} + \frac{N_O}{2}E_{O_2}}{2A} \quad (8)$$

where E_{Total}, $E_{Bulk}^{Fe_2O_3}$, E_{Bulk}^{Pd}, and E_{O_2} are the energies of the surface of interest, the bulk α-Fe_2O_3 system, a Pd atom in bulk fcc Pd, and molecular oxygen. Also, $N_{Fe_2O_3}$, N_{Pd}, N_O, and A are the number of α-Fe_2O_3 units in the surface, the number of Pd adsorbates, the number of oxygen vacancies created, and the surface area of the unit cell. The surface energies for all the surfaces studied here (complete and with a single oxygen vacancy) were calculated and are presented in Table 6.

Table 6. Calculated Surface Energies for the α-Fe_2O_3 (0001) Surfaces with Varying Pd Coverages Both Complete and with a Single Oxygen Vacancy

	Surface Energy (meV)		
system	0.0 ML Pd	0.5 ML Pd	1.0 ML Pd
complete	73.4	142.0	168.9
vacancy O-1	86.8	136.9	176.7
vacancy O-2	86.8	135.7	153.9

From the surface energy results, it is clear that the presence of surface Pd on the oxide initially destabilizes the complete Fe_2O_3 surfaces by increasing the surface energy by ~96 meV/Å^2 at the 1 ML Pd coverage case. As oxygen vacancies are created in the Fe_2O_3 surface, the surface energy of the clean Fe_2O_3 surface increases by ~13 meV/Å^2, which shows that the Fe surface becomes less stable as the surface oxygen are removed. However, the presence of Pd on the Fe_2O_3 surfaces stabilizes the reduced oxide surfaces relative to the complete Pd/Fe_2O_3 surfaces. Specifically, at the O-1 site, the 1/2 ML Pd coverage system shows that as a surface oxygen is removed, the surface energy decreases by ~5 meV/Å^2. While for the 1 ML Pd coverage system in the O-1 site the surface energy increases by ~8 meV/Å^2, which is consistent with the E_{rxn} results shown in Figure 9. Overall, these results show that the decrease in E_{rxn} with increasing Pd coverage up to 1/2 ML is likely due to the general stabilization effect that Pd has on the Fe_2O_3 surface due to the delocalization of the oxide surface electrons.

Second, for an oxygen vacancy created at site O-2, the vacancy reaction and oxygen bonding energies significantly decrease with increasing Pd surface coverage and the presence of surface Pd reduces the surface energy of the reduced oxide surface. Specifically, as the Pd coverage increases from 0 to 1 ML, the vacancy reaction and oxygen bonding energies decrease by 1.7 and 1.0 eV. The surface energy trends show that while the creation of an oxygen vacancy at site O-2 in the clean Fe_2O_3 surface decreases the stability of the surface by ~13 meV/Å^2, the surface energy decreases by ~6 meV/Å^2 and ~15 meV/Å^2 for the 1/2 and 1 ML Pd coverage systems relative to their complete Pd covered oxide surfaces. The surface energy results for the O-2 site are in agreement with the O-1 surface energy results which show that the presence of surface Pd on Fe_2O_3 stabilizes the reduced oxide surface. While the results for a vacancy created at the O-1 site showed that Pd facilitates the creation of oxygen vacancies through its general surface stabilization effect, the results for a vacancy created at the O-2 site suggests that the binding between surface oxygen and adsorbed Pd also weakens the bonds holding the oxygen within the oxide surface. Also, the creation of a second oxygen vacancy in the α-Fe_2O_3 (0001) surfaces with varying Pd coverages was studied, and the above thermodynamic trends were found to be true for the removal of the second oxygen as well (see the Supporting Information).

To further elucidate the effect of the Pd−O bonding on the creation of oxygen vacancies as seen in site O-2, we have calculated the PDOS (Figure 5b) and change in Bader charge relative to the complete oxide surfaces (Table 3) for the Fe, O, and Pd in the single oxygen vacancy α-Fe_2O_3 (0001) surfaces presented above (Figure 8). After an oxygen vacancy has been created at the O-2 site and the surfaces have been relaxed, it

dx.doi.org/10.1021/cs500565e | ACS Catal. 2014, 4, 3381−3392

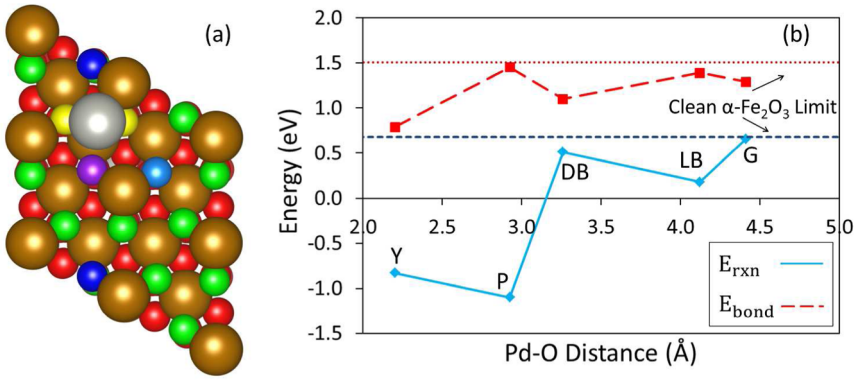

Figure 10. (a) Structure of the α-Fe_2O_3 (0001) surface with 1/8 ML Pd coverage and (b) the change in the vacancy formation energy (E_{rxn}) and surface oxygen bonding energy (E_{bond}) with the Pd−O distance. The general color coding for the structure is as in Figure 3 with the different surface oxygen sites identified with either green (G), yellow (Y), purple (P), light blue (LB), or dark blue (DB) spheres. Note that the unit cell in (a) has been expanded from the p(2 × 2) system for ease of viewing and the all edge atoms are repeated on the opposite edges due to the periodic boundary conditions.

was found that the remaining oxygen in the clean α-Fe_2O_3 (0001) surface were both symmetrically and electronically equivalent, while the two remaining surface oxygen in the Pd covered α-Fe_2O_3 (0001) surfaces were not symmetrically equivalent (see Figure S1). Furthermore, a comparison of the PDOS of the two oxygen showed that these two oxygens were electronically not equivalent. Therefore, the PDOS for the surface O with the smallest Pd−O bond distance was chosen for the PDOS analysis, as shown in Figure 5b. From the PDOS analysis (Figure 5b), it is clear that the removal of a single oxygen from the system further delocalizes the electrons in the surface, allowing them to move more easily between elements and energy levels and presenting a more metallic surface characteristic. This delocalization of electrons is constrained primarily to the surface metals (Fe and Pd), as shown in the changes of the Bader charge on these metals (Table 3). As the oxygen is removed, the surface metal elements gain electrons with an even distribution between the three exposed metals, while the surface oxygen shows no change in their Bader charge.

From the XPS results (Figure 6), the surface Pd has a limited range of effectiveness on the Fe_2O_3 surface. To model this and determine the Pd's effective range, the creation of oxygen vacancies in the α-Fe_2O_3 (0001) surface with a 1/8 ML Pd coverage was studied. For the model system, the 1/8 ML Pd coverage was created by increasing the model unit cell size to a p(2 × 2) supercell, and a single Pd was adsorbed onto one of the available O_B sites. The model system and resulting Pd distance effect is shown in Figure 10. The energetic analysis performed here was accomplished using eqs 6 and 7 to calculate the oxygen bonding energies and the overall reaction energies.

As the distance between the Pd and surface oxygen being removed increases, we see an increase in both the E_{rxn} and E_{bond} of the system toward the clean α-Fe_2O_3 (0001) surface limit. This is consistent with the experimental XPS results (Figure 6) which show that Pd only has an effect on the nearby surface's electronic structure. From Figure 10b, it is clear that oxygen within ∼3 Å of the adsorbed Pd will be significantly easier to remove, with an overall exothermic reaction energy, while those in the ∼3−4 Å Pd−O distance range will be mildly effected by Pd's stabilization effect, with a switch in the reaction energy from exothermic to endothermic. At Pd−O distances of greater than ∼4 Å, the creation of oxygen vacancies will be unaffected by Pd's stabilizing effect and behave like the clean Fe_2O_3 surface.

In addition to the work presented here, the presence of H_2 on the model oxide surfaces was studied, and the results are presented in the Supporting Information. Overall, it is clear that the presence of Pd on the Fe_2O_3 surface not only stabilizes the oxide and reduced oxide surfaces but also promotes the formation of water over hydroxyl groups. This result is consistent with work performed by Wang et al.[19] who showed that the formation of water from hydrogen and oxygen was significantly more energetically favorable on Pd single crystal surfaces as compared to Fe single crystal surfaces.

Thus far, our theoretical results show that the adsorption of Pd on the α-Fe_2O_3 (0001) surface decreases the energy required to form oxygen vacancies in said surface through two mechanisms, general surface stabilization and direct Pd−O bonding, and there is good qualitative agreement between the theoretical and experimental results. A greater degree of quantitative agreement between TPR and theory can be achieved by modeling the creation of oxygen vacancies using first order desorption kinetics[60,61] as defined by

$$\frac{d\theta}{dT} = -\frac{1}{\alpha} A\theta \exp\left(\frac{-V_o}{k_B T}\right) \quad (9)$$

where $d\theta/dT$ is the change in vacancy coverage within the first monolayer of the oxide with temperature, θ is the vacancy coverage, α is the heating rate (5 °C/min), A is the pre-exponential factor, V_o is the vacancy creation activation energy, k_B is Boltzmann's constant, and T is temperature. From the experimental conditions, we know that the temperature linearly increases with time at a constant heating rate (5 °C/min). With this model, we assume that the pre-exponential factor remains constant with temperature at 10^{13} s^{-1}. We solved this differential equation using a simultaneous fourth and fifth order Runge−Kutta method with variable step size and found that the experimental reduction temperatures for the Fe_2O_3 and Pd/Fe_2O_3 surfaces related to reduction energies of 1.62 and 1.25 eV, respectively, with an overall energy difference of 0.37 eV. These values are consistent with the oxygen bonding energies predicted from theory using DFT+U, where the Fe_2O_3 and 1/2 ML Pd/Fe_2O_3 surfaces resulted in oxygen bond

dx.doi.org/10.1021/cs500565e | ACS Catal. 2014, 4, 3381−3392

energies of 1.38 and 0.62 eV (Figure 9), respectively, with an energy difference of 0.72 eV. These energies show that there is good qualitative agreement between theory and experiment, even with these simplified models.

Overall, we have shown here that there is a strong quantitative agreement between experimentally and theoretically determined oxygen bond energies in the Pd/Fe_2O_3 system. Our work shows that the presence of Pd on the Fe_2O_3 surface delocalizes the oxide surface electrons. This electron delocalization stabilizes the reduced Fe_2O_3 surface and significantly decreases the energy required to reduce the oxide surface to within a ~4 Å radius of the surface Pd atom, which agrees with the XPS results showing the Pd has a limited range of effect. The addition of H_2 to the surface does not alter our findings from the clean Pd/Fe_2O_3 system but shows that the presence of Pd on the oxide surface stabilizes the formation of H_2O molecules over surface hydroxyl groups (Supporting Information). Therefore, the presence of Pd on the Fe_2O_3 surface enhances the reducibility of that surface by promoting the formation of water and by delocalizing the electrons within the oxide surface, stabilizing the reduced Fe surface. This stabilization of the reduced Fe surface by surface Pd likely protects the Fe surface from oxidation during the HDO reaction.

4. CONCLUSIONS

We have presented a combination of experimental and theoretical work concerning the effect of Pd on the reducibility of Fe_2O_3. Both our TPR and theoretical work show that the addition of Pd to the Fe_2O_3 surface results in a significant decrease in the energy required to reduce the oxide surface. From the XPS and theoretical studies, the interaction between Pd and the surface of Fe_2O_3 was found to occur through electron exchange between the topmost Fe and O elements with the preferential Pd binding sites occurring in sites with smallest Pd−O bond lengths. This surface Pd was found to partially donate electrons to the topmost surface Fe which allowed the oxide surface electrons to become more delocalized as seen in the appearance of O and Fe states in the original Fe_2O_3 band gap. The delocalization of surface oxide electrons resulted in the stabilization of the reduced oxide surface when surface Pd was present. Based on these results, it is likely that a significant portion of the synergistic effect found in the Pd/Fe_2O_3 catalyst is due to Pd's protection of the active metallic Fe from oxygen poisoning through the facilitated reduction of FeO_x species and promotion of water formation.

■ ASSOCIATED CONTENT

Supporting Information

Text describing the procedure used to calculate the core level binding energy shifts for the Pd 3d, Fe 2p, and O 1s orbitals in the 1/2 ML Pd covered α-Fe_2O_3 (0001) surface, the results for the creation of a second oxygen vacancy in the Pd covered α-Fe_2O_3 (0001) surfaces, and the calculated structural and energetic analysis of the α-Fe_2O_3 (0001) and 1/2 ML Pd covered α-Fe_2O_3 (0001) surfaces with a single H_2 molecule present on the surface. This material is available free of charge via the Internet at http://pubs.acs.org.

■ AUTHOR INFORMATION

Corresponding Authors

*Phone: 509-335-8580. Fax: 509-335-4806. E-mail: js.mcewen@wsu.edu (J.-S.M.).

*Phone: 509-371-6273. E-mail: yong.wang@pnnl.gov (Y.W.).

Author Contributions

[+]These authors (A.J.R.H. and Y.H.) contributed equally to this work.

Notes

The authors declare no competing financial interest.

■ ACKNOWLEDGMENTS

We acknowledge the financial support from the US Department of Energy (DOE), Office of Basic Energy Sciences, Division of Chemical Sciences, Geosciences, and Biosciences. This work was also supported by institutional funds provided to J.S.M. from the Voiland School of Chemical Engineering and Bioengineering. We thank the Franceschi Microscopy and Imaging Center (FMIC) in Washington State University for the access to their TEM. A portion of the research was performed using EMSL, a national scientific user facility sponsored by the Department of Energy's Office of Biological and Environmental Research and located at Pacific Northwest National Laboratory. We would also like to acknowledge Dr. Mark Engelhard at EMSL for his XPS measurement contributions. Finally, we acknowledge computational resources provided by the Center for Nanoscale Materials at Argonne National Laboratory. Use of the Center for Nanoscale Materials was supported by the U.S. Department of Energy, Office of Science, and Office of Basic Energy Sciences under Contract No. DE-AC02-06CH11357.

■ REFERENCES

(1) Ragauskas, A.; Williams, C.; Davison, B.; Britovsek, G.; Cairney, J.; Eckert, C.; Frederick, W.; Hallet, J.; Leak, D.; Liotta, C.; Mielenz, J.; Murphy, R.; Templer, R.; Tschaplinski, T. *Science* **2006**, *311*, 484−489.

(2) Lovins, A. B.; Datta, E. K.; Bustnes, O.-E.; Koomey, J. G.; Glasgow, N. J. In *Winning the Oil Endgame: Innovation for Profits, Jobs, and Security*; Rocky Mountain Institute: 2005.

(3) Mohan, D.; Pittman, C. U.; Steele, P. H. *Energy Fuels* **2006**, *20*, 848−889.

(4) Wang, H.; Male, J.; Wang, Y. *ACS Catal.* **2013**, *3*, 1047−1070.

(5) Maggi, R.; Delmon, B. *Biomass Bioenergy* **1994**, *7*, 245−249.

(6) Laurent, E.; Delmon, B. *Appl. Catal., A* **1994**, *109*, 77−96.

(7) Laurent, E.; Delmon, B. *Appl. Catal., A* **1994**, *109*, 97−115.

(8) Odebunmi, E. O.; Ollis, D. F. *J. Catal.* **1983**, *80*, 56−64.

(9) Odebunmi, E. O.; Ollis, D. F. *J. Catal.* **1983**, *80*, 65−75.

(10) Odebunmi, E. O.; Ollis, D. F. *J. Catal.* **1983**, *80*, 76−89.

(11) Ratcliff, M. A.; Johnson, D. K.; Posey, F. L.; Chum, H. L. *Appl. Biochem. Biotechnol.* **1988**, *17*, 151−160.

(12) Olcese, R. N.; Bettahar, M.; Petitjean, D.; Malaman, B.; Giovanella, F.; Dufour, A. *Appl. Catal., B* **2012**, *115−116*, 63−73.

(13) Olcese, R.; Bettahar, M. M.; Malaman, B.; Ghanbaja, J.; Tibavizco, L.; Petitjean, D.; Dufour, A. *Appl. Catal., B* **2013**, *129*, 528−538.

(14) Sun, J; Karim, A. M.; Zhang, H.; Kovarik, L.; Li, X.-H. S.; Hensley, A. J.; McEwen, J.-S.; Wang, Y. *J. Catal.* **2013**, *306*, 47−57.

(15) Hensley, A. J.; Zhang, R.; Wang, Y.; McEwen, J.-S. *J. Phys. Chem. C* **2013**, *117*, 24317−24328.

(16) Nørskov, J.; Bligaard, T.; Logadottir, A.; Bahn, S.; Hansen, L. B.; Bollinger, M.; Bengaard, H.; Hammer, B.; Sljivancanin, Z.; Mavrikakis, M.; Xu, Y.; Dahl, S.; Jacobsen, C. J. H. *J. Catal.* **2002**, *209*, 275−278.

(17) Nie, L.; de Souza, P. M.; Noronha, F. B.; An, W.; Sooknoi, T.; Resasco, D. E. *J. Mol. Catal. A: Chem.* **2014**, *388−389*, 47−55.

(18) Christmann, K. *Surf. Sci. Rep.* **1988**, *9*, 1−163.

(19) Wang, S.; Petzold, V.; Tripkovic, V.; Kleis, J.; Howalt, J. G.; Skúlason, E.; Fernández, E. M.; Hvolbæk, B.; Jones, G.; Toftelund, A.; Falsig, H.; Björketun, M.; Studt, F.; Abild-Pedersen, F.; Rossmeisl, J.;

Nørskov, J. K.; Bligaard, T. *Phys. Chem. Chem. Phys.* **2011**, *13*, 20760−20765.
(20) Wang, H.-F.; Gong, X.-Q.; Guo, Y.-L.; Guo, Y.; Lu, G. Z.; Hu, P. *J. Phys. Chem. C* **2009**, *113*, 10229−10232.
(21) Shapovalov, V.; Metiu, H. *J. Catal.* **2007**, *245*, 205−214.
(22) Li, B.; Metiu, H. *J. Phys. Chem. C* **2010**, *114*, 12234−12244.
(23) Kim, H. Y.; Lee, H. M.; Pala, R. G. S.; Shapovalov, V.; Metiu, H. *J. Phys. Chem. C* **2008**, *112*, 12398−12408.
(24) Pala, R. G. S.; Metiu, H. *J. Phys. Chem. C* **2007**, *111*, 8617−8622.
(25) Lebedeva, O. E.; Sachtler, W. M. H. *J. Catal.* **2000**, *191*, 364−372.
(26) Xu, G.-P.; Zhu, Y.-X.; Ma, J.; Yan, H.-J.; Xie, Y.-C. *Stud. Surf. Sci. Catal.* **1997**, *112*, 333−338.
(27) Belousov, V. M.; Vasylyev, M. A.; Lyashenko, L. V.; Vilkova, N. Y.; Nieuwenhuys, B. E. *Chem. Eng. J.* **2003**, *91*, 143−150.
(28) Li, S.; Meitzner, G. D.; Iglesia, E. *Stud. Surf. Sci. Catal.* **2001**, *136*, 387−392.
(29) Brunauer, S.; Emmett, P. H.; Teller, E. *J. Am. Chem. Soc.* **1938**, *60*, 309−319.
(30) Barrett, E. P.; Joyner, L. G.; Halenda, P. P. *J. Am. Chem. Soc.* **1951**, *73*, 373−380.
(31) Kresse, G.; Hafner, J. *Phys. Rev. B* **1993**, *47*, 558−561.
(32) Kresse, G.; Furthmueller, J. *Phys. Rev. B* **1996**, *54*, 11169−11186.
(33) Rollmann, G.; Rohrbach, A.; Entel, P.; Hafner, J. *Phys. Rev. B* **2004**, *69*, 165107/1−165107/12.
(34) Dudarev, S. L.; Botton, G. A.; Savrasov, S. Y.; Humphreys, C. J.; Sutton, A. P. *Phys. Rev. B* **1998**, *57*, 1505−1509.
(35) Kiejna, A.; Pabisiak, T. *J. Phys.: Condens. Matter* **2012**, *24*, 095003/1−095003/16.
(36) Rohrbach, A.; Hafner, J.; Kresse, G. *Phys. Rev. B* **2004**, *70*, 125426/1−125426/17.
(37) Grau-Crespo, R.; Al-Baitai, A. Y.; Saadoune, I.; De Leeuw, N. H. *J. Phys.: Condens. Matter* **2010**, *22*, 255401/1−255401/7.
(38) Dong, C.; Sheng, S.; Qin, W.; Lu, Q.; Zhao, Y.; Wang, X.; Zhang, J. *Appl. Surf. Sci.* **2011**, *257*, 8647−8652.
(39) Souvi, S. M. O.; Badawi, M.; Paul, J.-F.; Cristol, S.; Cantrel, L. *Surf. Sci.* **2013**, *610*, 7−15.
(40) Kresse, G.; Joubert, D. *Phys. Rev. B* **1999**, *59*, 1758−1775.
(41) Perdew, J. P.; Wang, Y. *Phys. Rev. B* **1992**, *45*, 13244−13249.
(42) Vosko, S. H.; Wilk, L.; Nusair, M. *Can. J. Phys.* **1980**, *58*, 1200−1211.
(43) Monkhorst, H. J.; Pack, J. D. *Phys. Rev. B* **1976**, *13*, 5188−5192.
(44) Stevens, E. D.; Rys, J.; Coppens, P. *J. Am. Chem. Soc.* **1978**, *100*, 2324−2328.
(45) Condon, N. G.; Murray, P. W.; Leibsle, F. M.; Thornton, G.; Lennie, A. R.; Vaughan, D. J. *Surf. Sci.* **1994**, *310*, L609−L613.
(46) Meng, X. Y.; Qin, G. W.; Li, S.; Wen, X. H.; Ren, Y. P.; Pei, W. L.; Zuo, L. *Appl. Phys. Lett.* **2011**, *98*, 112104/1−112104/3.
(47) Sartoretti, C. J.; Alexander, B. D.; Solarska, R.; Rutkowska, I. A.; Augustynski, J.; Cerny, R. *J. Phys. Chem. B* **2005**, *109*, 13685−13692.
(48) Bader, R. F. W. In *Atoms in Molecules: A Quantum Theory*; Oxford University Press: Oxford, 1990.
(49) Zhang, R.; Hensley, A. J.; McEwen, J.-S.; Wickert, S.; Darlatt, E.; Fischer, K.; Schöppke, M.; Denecke, R.; Streber, R.; Lorenz, M.; Papp, C.; Steinrück, H. P. *Phys. Chem. Chem. Phys.* **2013**, *15*, 20662−20671.
(50) Köhler, L.; Kresse, G. *Phys. Rev. B* **2004**, *70*, 165405/1−165405/9.
(51) Fischer, A.; Krozer, A.; Schlapbach, L. *Surf. Sci.* **1992**, *269−270*, 737−742.
(52) Bhat, V. V.; Contescu, C. I.; Gallego, N. C. *Nanotechnology* **2009**, *20*, 204011/1−204011/10.
(53) Zieliński, J.; Zglinicka, I.; Znak, L.; Kaszkur, Z. *Appl. Catal., A* **2010**, *381*, 191−196.
(54) Cai, L.-L.; Lu, G.-Z.; Zhan, W.-C.; Guo, Y.; Guo, Y.-L.; Yang, Q.-S.; Zhang, Z.-G. *J. Mater. Sci.* **2011**, *46*, 5639−5644.
(55) Liu, J.; Sun, B.; Hu, J.-Y.; Pei, Y.; Li, H.-X.; Qiao, M.-H. *J. Catal.* **2010**, *274*, 287−295.
(56) Yang, T.-Y.; Kang, H.-Y.; Sim, U.; Lee, Y.-J.; Lee, J.-H.; Koo, B.; Nam, K. T.; Joo, Y.-C. *Phys. Chem. Chem. Phys.* **2013**, *15*, 2117−2124.
(57) Xiao, C.; Liang, M.-H.; Gao, A.; Xie, J.-L.; Wang, Y.; Liu, H.-C. *J. Nanopart. Res.* **2013**, *15*, 1822/1−1822/11.
(58) Yin, S.-X.; Ellis, D. E. *Surf. Sci.* **2008**, *602*, 2047−2054.
(59) Chen, Z.-Q.; Cvelbar, U.; Mozetic, M.; He, J.-Q.; Sunkara, M. K. *Chem. Mater.* **2008**, *20*, 3224−3228.
(60) Parker, D. H.; Jones, M. E.; Koel, B. E. *Surf. Sci.* **1990**, *233*, 65−74.
(61) Kreuzer, H. J.; Payne, S. H. In *Theories of the Adsorption-Desorption Kinetics on Homogeneous Surfaces in Equilibria and Dynamics of Gas Adsorption on Heterogeneous Solid Surfaces*; Rudzin, W., Steele, W. A., Zgrablich, G., Eds.; Elsevier: 1997.